

# Implementation of time-dependent Hartree Fock in real space

**Uday Panta**

Department of Physics, University of California, Merced, 5200 N. Lake Rd., Merced, CA 95343, USA

**David A. Strubbe**

Department of Physics, University of California, Merced, 5200 N. Lake Rd., Merced, CA 95343, USA

E-mail: [dstrubbe@ucmerced.edu](mailto:dstrubbe@ucmerced.edu)

## Abstract.

Time-dependent Hartree-Fock (TDHF) is one of the fundamental post-Hartree-Fock (HF) methods to describe excited states. In its Tamm-Dancoff form, equivalent to Configuration Interaction Singles, it is still widely used and particularly applicable to big molecules where more accurate methods may be unfeasibly expensive. However, it is rarely implemented in real space, mostly because of the expensive nature of the exact-exchange potential in real space. Compared to widely used Gaussian-type orbitals (GTO) basis sets, real space often offers easier implementation of equations and more systematic convergence of Rydberg states, as well as favorable scaling, effective domain parallelization, flexible boundary conditions, and ability to treat model systems. We implemented TDHF in the Octopus real-space code as a step toward linear-response hybrid time-dependent density-functional theory (TDDFT), other post-HF methods, and ensemble density-functional theory methods involving exact exchange. Calculation of HF's non-local exact exchange is very expensive in real space. We overcome this limitation with Octopus' implementation of Adaptively Compressed Exchange (ACE), and find the appropriate mixing and starting point to complete the ground-state calculation in a practical amount of time, to enable TDHF. We compared our results to those from GTOs on a set of small molecules and confirmed close agreement of results, though with larger deviations than in the case of semi-local TDDFT. We find that convergence of TDHF demands a finer real-space grid than semi-local TDDFT. We also present the subtleties in benchmarking a real-space calculation against GTOs, relating to Rydberg and vacuum states.

## 1. Introduction

Hartree-Fock (HF) theory [1, 2] is a main pillar in quantum chemistry, serving as the starting point for calculating the electronic structure of molecules. HF calculations provide molecular geometry, electron distribution, and ground-state properties [3]. Once the ground state has been calculated, excited states can be calculated using the ground-state results. A first approximation one can make for the excitation energies is from the eigenvalue differences of the unoccupied and occupied states, termed the Independent Particle Approximation (IPA) [4]. Configuration Interaction (CI), Equation-of-Motion Coupled Cluster (EOM-CC), and Time-Dependent Hartree-Fock (TDHF) are examples of post-Hartree-Fock methods [5] that can

provide more accurate excited states. The exact exchange potential used in HF is orbital-dependent while it is density-dependent in traditional semi-local Kohn-Sham Density Functional Theory (DFT). Hybrid functionals which are a mixture of these two types of exchange potentials are widely used [6, 7, 8] to improve accuracy, so TDHF is a building block for time-dependent density-functional theory (TDDFT) with hybrids.

Hartree-Fock theory provides a reasonably accurate description of the ground state of molecular systems, especially for small-to-moderately sized molecules and systems where electron correlation effects are not dominant [9]. Gaussian-type orbitals (GTOs) are typically used as basis sets for Hartree-Fock [10]. Implementation of Hartree-Fock in real space is rare, though a finite-element-type implementation has been published [11]. Using GTOs conveniently allows integrals to be done analytically. However, the nature of orbitals one can obtain in an electronic structure calculations heavily depends on the type and size of the basis set used. The basis set is typically optimized for the ground state which can make description of unoccupied orbitals difficult [12]. This issue is particularly acute for Rydberg states which are highly excited states that are far from the atoms and weakly bound [13], but transitions from valence to Rydberg states can be important in optical properties [14]. To include these states, additional diffuse functions is added to the basis sets [15]. Comparisons of GTOs and real space have shown that such very large, diffuse basis sets can be needed to describe the excited states involved in non-linear optical response [16]. In real space, Rydberg states do not require special diffuse functions but can be captured by systematically converging the physical size of the real-space domain in which the orbitals are calculated. the number of grid-points which can be systematically converged [17]. Other advantages of real-space calculations include favorable scaling for large systems, effective parallelization over domains, and straightforward use of both finite and periodic boundary conditions [17, 18, 19], and ability to handle non-atomic model systems [20]. In real-space however, the calculation of exchange integrals becomes very expensive [21] and these integrals are a major part of any HF calculation underlying TDHF.

In this paper, we present our results from our real-space implementation of TDHF in the Octopus code. In section 2, we discuss the general theory behind ground-state HF and TDHF. Section 3.1 discusses the exact exchange potential which is the main feature of HF which sets it apart from traditional Kohn-Sham DFT. As this is the most expensive part of the calculation, we discuss a formalism, ACE, which has been available in Octopus for a while now for hybrid DFT calculations to speed up the exact exchange calculation. We also present the general parameters used in our calculations and the need for them in sections 3.3 and 3.4. In section 4 we discuss the general difficulties in reaching a solution to the HF ground-state in real-space and how to overcome them. Finally, section 4.5 shows the comparison of excitation energies obtained from GTO-based approach to the real-space approach, demonstrating a good level of agreement and practical attainability of convergence with respect to the real-space grid parameters.

## 2. Theory

Ground-state HF calculations involve solving for energy eigenvalues  $\epsilon_i$  and eigenstates  $\{\psi_i\}$  with a self-consistent field (SCF) calculation via the Hartree-Fock-Roothan equations [22]:

$$\left( -\frac{1}{2}\nabla^2 + V_{\text{ion}} + V_{\text{H}}[\rho] + \hat{V}_{\text{X}}[\{\psi_j\}] \right) \psi_i = \epsilon_i \psi_i \quad (1)$$

The four terms in the bracket are kinetic energy operator, external potential, Hartree potential, and exchange potential. The Hartree potential depends on the density  $\rho(r) = \sum_j^{N_e} |\psi_j|^2$ , where  $N_e$  is the number of electrons. The exchange potential takes the form of exact exchange and its

action on an arbitrary orbital  $\psi_p$  is given by

$$\hat{V}_X[\{\psi_j\}]\psi_p(r) = -\sum_{j=1}^{N_e} \psi_j(r) \int \frac{\psi_j(r')\psi_p(r')}{|r-r'|} dr'. \quad (2)$$

Correlation is absent, unlike DFT which has the exchange-correlation functional  $V_{XC}$ . To calculate the excited-state properties of a system in most linear-response methods, we need extra unoccupied (virtual) orbitals. Self-consistency is not required here because the unoccupied orbitals do not contribute to the density or exchange potential of the system.

TDHF can be applied in a real-time propagation form like in TDDFT [23], but we focus here on its linear-response matrix form. It has a similar structure to linear-response TDDFT, as an equation for excitation-energy eigenvalues  $\omega$  and eigenvectors with excitation component  $X$  and de-excitation component  $Y$ , and block matrices  $A$  and  $B$  [9]:

$$\begin{bmatrix} \mathbf{A} & \mathbf{B} \\ -\mathbf{B} & -\mathbf{A} \end{bmatrix} \begin{bmatrix} \mathbf{X} \\ \mathbf{Y} \end{bmatrix} = \omega \begin{bmatrix} \mathbf{1} & \mathbf{0} \\ \mathbf{0} & \mathbf{1} \end{bmatrix} \begin{bmatrix} \mathbf{X} \\ \mathbf{Y} \end{bmatrix}. \quad (3)$$

The matrix elements in the case of a spin-polarized (unrestricted HF, UHF) calculation are given by

$$A_{ia,jb} = \delta_{ij}\delta_{ab}(\epsilon_a - \epsilon_i) + (ia||jb) \quad (4)$$

and

$$B_{ia,jb} = (ia||bj) \quad (5)$$

where  $i, j$  represent occupied orbitals and  $a, b$  represent unoccupied orbitals. Here the shorthand notation  $(pq||rs) = (pq|rs) - (pr|qs)$  has been used where

$$(pq|rs) = \int \frac{d^3\mathbf{r}'d^3\mathbf{r}}{|\mathbf{r}-\mathbf{r}'|} \phi_p^*(\mathbf{r}')\phi_q(\mathbf{r}')\phi_r^*(\mathbf{r})\phi_s(\mathbf{r}).$$

For spin-unpolarized (restricted HF, RHF) calculations, the matrix elements are given by [22]

$$A_{ia,jb} = \delta_{ij}\delta_{ab}(\epsilon_a - \epsilon_i) + \delta_M(ai||jb) - (ab||ji) \quad (6)$$

where  $\delta_M = 2$  and  $0$  for singlets and triplets respectively.

This full TDHF formulation in equation 3 is a non-Hermitian eigenvalue problem, with matrix size twice the number of transitions considered. For real orbitals, the equation can be transformed into a Hermitian problem of half the matrix size [24]. One widely used approximation (applicable for complex orbitals too) is neglecting the matrix  $B$  in to equation 3 completely and only solving for  $AX = \omega X$ , which is again a Hermitian problem of half the matrix size. This Tamm-Dancoff approximation (TDA) not only makes the calculation less computationally intensive but also has been shown to perform better than full TDHF [25]. It is equivalent to Configuration Interaction Singles (CIS) [9]. While TDA has been known to underestimate the transition dipole moments [26] compared to the full TDHF, it gives good estimate of the excitation energies and molecular properties [27]. Neglecting the exchange and Hartree integrals in equation 6 and calculating the excitation energy as the difference of virtual and occupied eigenvalues is the IPA. This work will focus on TDA-TDHF, adapting Octopus' existing implementation [19] of the transformed TDDFT equations for real orbitals (Casida equations) [24] and of Tamm-Dancoff TDDFT [28].

Once the TDHF eigenvalue problem is solved, one can obtain the absorption spectrum too. Using the TDA eigenvectors  $\{x_{k,ia}\}$ , the many-body dipole transition matrix elements reduce to a linear combination of single-particle matrix elements [22]:

$$\vec{d}_k = \sum_{ia} \langle i|\vec{r}|a\rangle x_{k,ia} \quad (7)$$

like in TDDFT, where the index  $ia$  runs over the pairs of occupied-unoccupied orbitals. The isotropically averaged oscillator strength is then calculated as

$$f_k = \frac{2m_e}{3\hbar^2} \omega_k |\vec{d}_k|^2 \quad (8)$$

The absorption spectrum for unpolarized light is represented by the strength function:

$$S(\omega) = \sum_k f_k \delta(\omega - \omega_k) \quad (9)$$

The  $\delta$  function is in practice broadened for plotting with a Lorentzian or Gaussian function.

### 3. Implementation

#### 3.1. Exchange Potential and Adaptively Compressed Exchange (ACE)

Unlike semi-local exchange and correlation density functionals such as the Local Density Approximation (LDA) [29, 30], the Hartree-Fock exchange potential is dependent on the molecular orbitals (equation 2) instead of the density. The non-local nature of this integral makes it time-consuming to solve numerically, especially in methods with large basis sets. Therefore real-space and plane-wave implementations use iterative algorithms which only require the application of  $\hat{V}_X$  to specific orbitals instead of the full construction of the operator  $\hat{V}_X$ .

Equation 2 can be solved as a Poisson equation with  $\rho(r) = \psi_j(r)\psi_i(r)$ , using various optimized Poisson solvers such as interpolating scaling functions, like for the Hartree potential [31]. The cost of solving equation 2 by direct integration for each  $r$  is  $\mathcal{O}(N_\mu^2)$  while the cost of solving as a Poisson problem is  $\mathcal{O}(N_\mu \log N_\mu)$  where  $N_\mu$  is the number of grid points. This is a significant improvement, but exact exchange still remains considerably more computationally intensive than a semi-local functional.

Adaptively Compressed Exchange (ACE) [32] is an approach we will use which was introduced to speed up the calculation of exact exchange. This method was previously implemented in Octopus. Other approaches available to speed up the exchange calculation include the Selected Column Density Matrix [33] and Recursive Subspace Bisection [21] methods. In the ACE formalism, the full-rank exchange operator,  $\hat{V}_X$ , is approximated by the low rank ACE operator,  $\hat{V}_X^{\text{ACE}} = \zeta\zeta^T$ , which is obtained iteratively as follows.

For ground-state SCF, we start with a guess of the exchange operator calculated using equation 2:

$$W_i(r) = (\hat{V}_X[\{\phi\}]\phi_i)(r) \quad (10)$$

for all  $\{\phi_i\}_{i=1}^{N_e}$ . Then matrix  $M$  is calculated using  $M_{kl} = \int \phi_k(r)W_l(r)dr$ . Cholesky factorization is performed on  $-M$  to get  $L$  such that  $M = -LL^T$ , where  $L$  is a lower triangular matrix. The projection vector in the ACE formulation is then calculated as

$$\zeta_k(r) = \sum_i^{N_e} W_i(r)(L^{-T})_{ik}. \quad (11)$$

Finally, we obtain the ACE operator as

$$\hat{V}_X^{\text{ACE}}(r, r') = - \sum_{k=1}^{N_e} \zeta_k(r) \zeta_k(r'). \quad (12)$$

ACE significantly reduces the cost of application of the exchange operator by reducing the prefactor but keeps the scaling with grid points the same as the scaling for LDA or HF without ACE [32]. Instead of calculating  $\hat{V}_X$  by integration from equation 2 for each iteration of the SCF cycle, ACE does it only once and improves it iteratively until the SCF density converges. After the self-consistency is reached, the action of  $\hat{V}_X^{\text{ACE}}$  on an orbital is the same as the action of  $\hat{V}_X$ . This significantly reduces the overall cost of computation because the cost of application of the exchange operator can often be more than 95% of the total cost in HF calculations.

Once the solution to the ground-state is achieved, we calculate a set of unoccupied orbitals via a non-self-consistent calculation. ACE is used here too with the only difference from the ground-state calculation being the inclusion of unoccupied orbitals in equations 10, 11 and 12. Although one can obtain these unoccupied orbitals in the ground-state SCF by calculating an extra set of eigenfunctions with zero occupation which do not contribute to the total energy, it is preferable to calculate the ground-state without unoccupied orbitals first, since calculation of these extra eigenfunctions in all iterations before convergence is not useful. The number of unoccupied orbitals one can obtain also depends on the size of the basis set: the number of eigenfunctions obtainable is equal to the size of the Hamiltonian matrix. Hence, the number of unoccupied orbitals obtainable from GTOs will be lower than that obtainable from the (orders of magnitude) larger number of real-space grid points. Usually, one calculates all possible unoccupied orbitals with GTOs, but in real space only a small fraction of the possible unoccupied orbitals are calculated.

ACE calculates the ground-state exchange potential iteratively as a whole by reducing the number times the exchange matrix is calculated in the SCF cycle. It is not implemented yet in Octopus to calculate individual exchange integrals with ACE, as would be needed for its use in TDHF. Refs. [34, 35] have shown this is possible with plane-waves and Gaussian basis sets using discrete variable representation [36] schemes. Whether this provides any speedup in real-space is yet to be studied and is a subject of future work. SCF, without ACE, requires solving  $N_e^2$  integrals for each iteration. However TDA-TDHF requires solving  $N_e N_{\text{unocc}}$  integrals only once to create the TDHF matrix which is diagonalized. This means the prefactor for TDHF integrals is generally lower than that for the SCF problem, and so it is more necessary to reduce the cost of exchange in SCF than in TDHF.

### 3.2. Mixing in SCF cycle

The nonlocality of the exchange potential makes different and more difficult SCF convergence behavior than in DFT. To facilitate faster convergence, different quantities can be mixed together from consecutive iterations and be used in the next iteration. The quantity that is usually mixed is the density, but one can also mix the potential or the wavefunctions. It should also be noted that mixing non-local potential is not as straightforward as mixing local potentials. In our calculations, we mix only the local part of the potential, i.e. the Hartree potential  $V_H$ .

The simplest mixing scheme is the linear mixing where a certain fraction of the quantity from the last SCF iteration  $N - 1$  is mixed with that from the current iteration  $N$ :

$$q_{N+1}(r) = \alpha q_{N-1}(r) + (1 - \alpha) q_N(r) \quad (13)$$

where  $q$  refers to the quantity that is being mixed and  $\alpha$  is called the ‘‘mixing parameter.’’ More sophisticated schemes like Broyden mixing [37, 38] and Pulay mixing [39] are widely used too.

### 3.3. Pseudopotentials

In real-space or plane-wave calculations, pseudopotentials (PPs) are the standard approach to account for the core electrons of a system only implicitly, which can be done because the core electrons usually do not take part in bonding or electronic and optical properties. In real-space, PPs also solve a crucial problem. The  $-Z/r$  Coulomb potential is divergent at  $r = 0$  and makes the wavefunctions vary very rapidly near the nucleus, requiring an infeasible large number of grid points to describe. PPs circumvent this problem [17]. In Gaussian basis sets, usually all the electrons are treated explicitly, except for heavy elements in which case effective core potentials [40] are used, which are a form of PPs. PPs are generated from all-electron calculations for a given DFT functional. Typically only local or semi-local functionals are used. Approaches to generate PPs for HF have been developed [41, 42] but such PPs are rarely used in practice [43] and are not supported by Octopus. In this paper, we use optimized norm-conserving Vanderbilt [44] scalar relativistic pseudopotentials from pseudo-dojo [45]. We use LDA [29, 30] pseudopotentials for all HF ground-state calculations, as well as the LDA calculations reported later. For DFT calculations with BLYP [46, 47] for our TDDFT comparison, we have used PBE PPs as BLYP and PBE are both GGA functionals and pseudo-dojo currently doesn't have BLYP PPs. For these TDDFT calculations, we note that Octopus currently only supports LDA kernels and so the LDA kernel [29, 30] is used for our TDDFT calculations based on a BLYP ground state.

Using PPs generated with one functional for a DFT calculation with a different functional is a common practice in DFT, and ubiquitous for hybrid functionals. A recent study shows that the inconsistent use of PPs does not make very significant differences [48] in DFT. In our study, although we are doing HF calculations, HF exchange is only applied to the valence electrons and not to the core electrons.

### 3.4. Real-space calculations

In the Octopus code [18, 19, 49], all quantities are represented on a grid in real space. The domain is divided into a grid, with zero boundary conditions applied on the surface. The default (“minimal”) simulation domain for molecules is a union of spheres centered around each atom. However, for the results presented in this paper, we have used a single big sphere that encapsulates the entire molecule. For all the molecules used in this work, the atoms would fit in a sphere of radius  $R = 3 \text{ \AA}$ , so for sphere radii much larger than that, the union-of-spheres domain is not very different from a single sphere. The radius of the encapsulating sphere used for benchmarking results is  $10 \text{ \AA}$  and a spacing  $h = 0.1 \text{ \AA}$  is used. These parameters, which define the real-space grid, can be converged systematically. In our case, they were selected by convergence tests of not only occupied but also unoccupied orbitals, as shown in section 4.4, since convergence of unoccupied orbitals is very important for excited-state calculations. We use 51 unoccupied orbitals for each molecule. The conjugate-gradients eigensolver was used, with a tolerance of  $10^{-6}$  eV. By default, Octopus uses as SCF convergence criterion the relative density error which measures the relative change of electron density between iterations as given by the following equation:

$$\epsilon = \frac{1}{N_e} \int |\rho^{\text{in}} - \rho^{\text{out}}| d^3r \tag{14}$$

where  $\rho^{\text{in}}$  and  $\rho^{\text{out}}$  are the densities at two consecutive iterations. Requiring eigensolver convergence for each state as an additional convergence criterion in SCF led to density convergence several orders of magnitude better than the default threshold  $10^{-6}$  for the relative density error, which is related to the fact that the HF Hamiltonian depends directly on the wavefunctions, not just the density.

## 4. Results

### 4.1. Speed-up of HF with ACE

To test the efficiency of the ACE formalism, we can look at the average time required to complete one iteration in the SCF cycle. Table 1 shows that the time per iteration for LDA calculations is 1 – 3% of the time per iteration for HF calculations without ACE, i.e. the direct solution of the Poisson equations for exchange. With ACE, however, we have achieved a speed up of at least 7 times, with maximum speed up of 14 times for formamide. We have also confirmed numerically identical results between calculations with and without ACE. We also studied the scaling of time per SCF iteration as a function of number of grid-points for LDA, HF without ACE, and HF with ACE, as shown in Figure 1. We see similar scaling in each case: the scaling should be  $\mathcal{O}(N_\mu)$  for LDA and  $\mathcal{O}(N_\mu \log N_\mu)$  for HF, which look similar on this scale. However, the speed up from ACE is dramatic. This is a big improvement in making the ground-state HF calculations practical: without ACE they were two orders of magnitude more expensive than LDA, but with ACE are only one order of magnitude more expensive.

| Molecule          | Time per SCF iteration (seconds)<br>(DFT-LDA) | Time per SCF iteration (seconds)<br>(HF) |          |          |
|-------------------|---|--|----------|----------|
|                   |   | Without ACE                              | With ACE | Speed up |
| acetaldehyde      | 0.19  | 20.27                                    | 1.71     | 11.85    |
| acetylene         | 0.05  | 3.41                                     | 0.42     | 8.14     |
| ammonia           | 0.05  | 2.12                                     | 0.28     | 7.59     |
| carbon monoxide   | 0.05  | 2.92                                     | 0.34     | 8.58     |
| cyclopropene      | 0.07  | 12.33                                    | 1.35     | 9.14     |
| diazomethane      | 0.08  | 11.12                                    | 1.12     | 9.93     |
| dinitrogen        | 0.05  | 2.57                                     | 0.34     | 7.68     |
| ethylene          | 0.05  | 5.12                                     | 0.66     | 7.76     |
| formaldehyde      | 0.12  | 10.62                                    | 1.09     | 9.71     |
| formamide         | 0.09  | 22.01                                    | 1.57     | 14.02    |
| hydrogen chloride | 0.04  | 1.88                                     | 0.26     | 7.33     |
| hydrogen sulphide | 0.05  | 2.08                                     | 0.27     | 7.68     |
| ketene            | 0.07  | 11.71                                    | 1.13     | 10.38    |
| methanimine       | 0.06  | 6.54                                     | 0.67     | 9.82     |
| nitrosomethane    | 0.07  | 22.34                                    | 1.64     | 13.61    |
| streptocyanine-cl | 0.10  | 20.88                                    | 1.97     | 10.63    |
| thioformaldehyde  | 0.06  | 6.25                                     | 0.66     | 9.46     |
| water             | 0.04  | 1.84                                     | 0.25     | 7.46     |

Table 1: Time per SCF iteration in different molecules. Times are calculated, on a node with two Intel 28 core Xeon Gold 6330 processors, by taking an average over the first 10 iterations for HF and an average over all iterations for LDA.

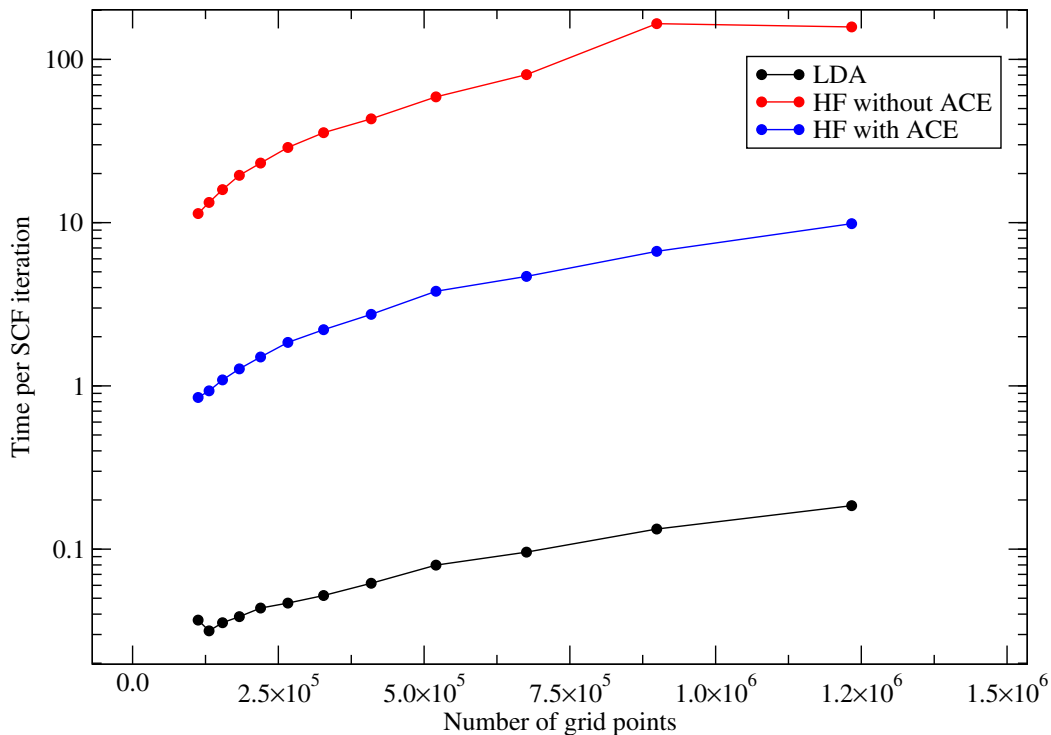


Figure 1: Scaling of time per SCF iteration for different approaches, showing similar scaling for each but an improved pre-factor for HF when using ACE. Times are calculated as an average for the first 20 SCF iterations for nitrosomethane molecule. Data obtained for fixed number of orbitals by varying grid spacing by  $0.01 \text{ \AA}$  from  $0.20 \text{ \AA}$  to  $0.09 \text{ \AA}$  on a simulation domain constructed from union of spheres of radii  $5 \text{ \AA}$  around each atom.

#### 4.2. Starting point for SCF convergence of HF

The ground-state SCF calculation can be difficult to converge for HF. The default initial guess in Octopus is a linear combination of atomic orbitals (LCAO) for the wavefunctions and a superposition of atomic densities for the density. One way to accelerate this convergence is to first calculate the ground-state using LDA (faster and more easily converged) and then use that as a starting point instead of using LCAO calculated in HF as the initial guess for the HF calculation, assuming that the convergence density will be similar. This approach is the standard recommendation in Octopus for hybrid functionals. To assess the convergence behaviour, we examine the relative density error as defined in equation 14.

Figure 2 shows the convergence characteristics of the SCF procedure for different starting guesses using Broyden density mixing. It is evident from Figure 2 that starting from LDA solution not only makes the convergence faster but is also responsible for any convergence at all as the HF from LCAO didn't converge within 300 iterations and was not making progress.



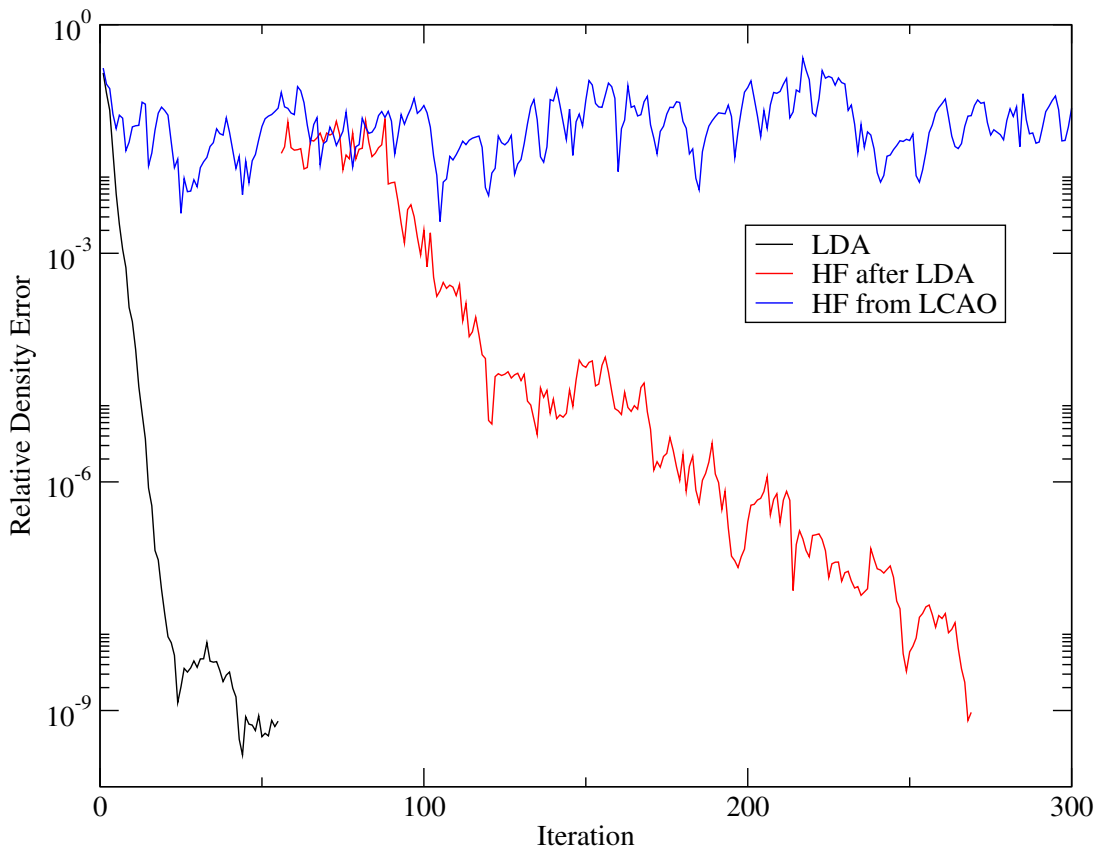


Figure 2: Convergence of HF ground-state for thioformaldehyde ( $h = 0.22 \text{ \AA}$ ,  $R = 5 \text{ \AA}$ ) from different starting points, measured by the relative density error defined in equation 14. First LDA calculation (black) was performed starting from a Linear Combination of Atomic Orbitals (LCAO) and the converged results were used as initial guess for HF calculation (red). The blue curve shows convergence when the HF calculation was performed directly from LCAO.

#### 4.3. Mixing for SCF convergence of HF

Figure 3 shows the convergence characteristics using different mixing quantities and mixing schemes for nitrosomethane at mixing parameters  $\alpha = 0.30$  and  $0.35$ . All HF calculations start using LDA solutions as initial guess. Although for LDA the Broyden scheme seems faster and smoother than linear mixing, HF doesn't converge at all with this scheme and linear mixing should be used to achieve convergence. For LDA, Broyden mixing of potential and density have similar behavior except that potential mixing provides smoother convergence at very low relative density error. For both LDA and HF, linear mixing of potential and density have similar behavior. The differences in all cases between our two values of  $\alpha$  is small whenever convergence is achieved. We also show the convergence character using linear mixing of states for the same system in Figure 4, showing significantly improved behavior. Mixing states seems the most robust strategy for faster convergence of SCF for a variety of molecules. This makes sense because the HF potential is not just a function of density but also of the orbitals, and converging orbitals should guarantee the convergence of both potential and density.

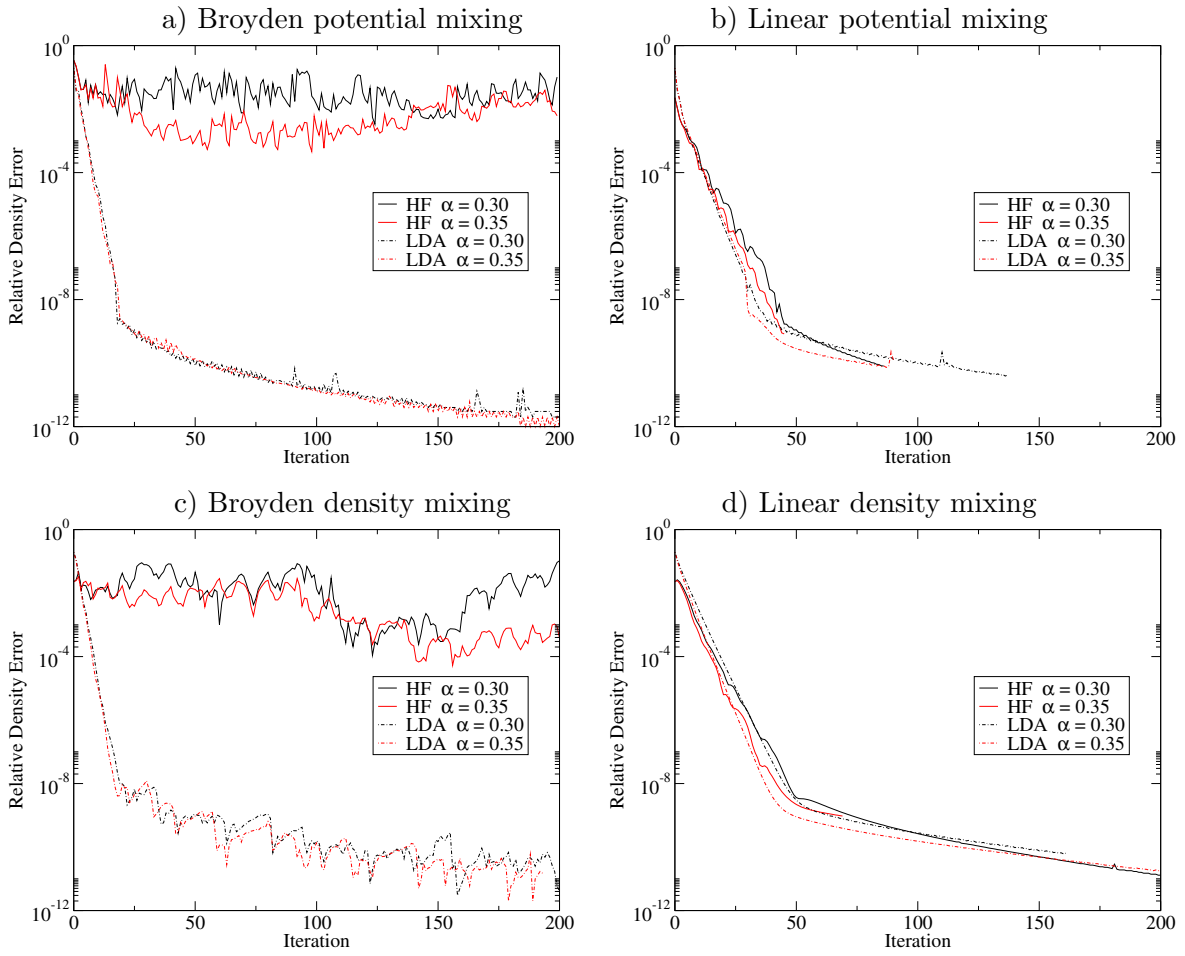


Figure 3: Effect of the mixing scheme, quantity being mixed, and the mixing parameter  $\alpha$  on convergence. The relative density error is defined in equation 14.

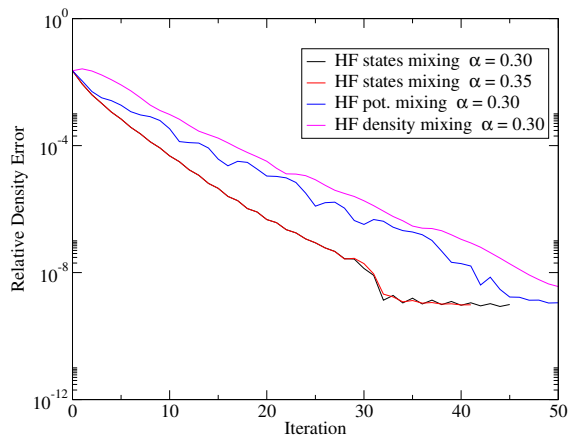


Figure 4: Convergence, as measured by the relative density error defined in equation 14, while mixing states (red and black with different mixing parameters) using linear scheme for the nitrosomethane molecule ( $h = 0.16 \text{ \AA}$ ,  $R = 5 \text{ \AA}$ ). Blue and magenta curves are linear mixing of potential and density respectively shown as a comparison to states mixing.

#### 4.4. Convergence of Orbitals with the Real-Space Grid Parameters

To obtain TDHF spectra converged with respect to the grid spacing  $h$  and sphere radius  $R$ , we must converge not only the ground-state density, but also the occupied and unoccupied orbitals' eigenvalues and wavefunctions. We show the convergence of occupied (Figure 5) and unoccupied (Figure 6) eigenvalues from HF and LDA with respect to the change in the grid spacing of the calculation domain.

The occupied orbitals converge within 0.01 eV at 0.14 Å for both LDA and HF, and have similar convergence behavior. The unoccupied orbitals similarly converge within 0.01 eV at 0.14 Å for LDA, but for HF a finer grid of spacing 0.1 Å is required to achieve the same level of convergence. This is not surprising since there is an additional integral to be converged in real space, in HF vs LDA. The occupied orbitals converge monotonically as the spacing is decreased in both LDA and HF. For unoccupied orbitals, this is the case for LDA too but not for HF. In Figure 7 we examine also the convergence of occupied eigenvalues with respect to the sphere radius  $R$ , which shows that eigenvalues are very well converged by  $R = 10$  Å. This is as expected since that large radius was chosen to ensure adequate description of the unoccupied orbitals. It is not straightforward to make a meaningful assessment of unoccupied eigenvalues' convergence with radius, because the state of a given index will continually decrease toward zero as the radius is increased, and converge only to zero. These vacuum states behave similarly to the particle-in-a-box model. Therefore we do not provide a plot of unoccupied states' convergence with radius. Overall we conclude that convergence of HF unoccupied orbitals is harder in real space but still achievable.

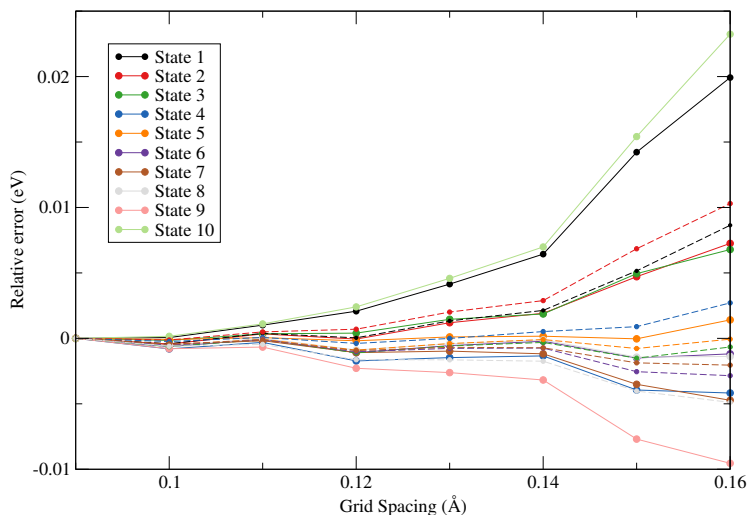


Figure 5: Relative error of the occupied orbitals' eigenvalues compared to the finest grid ( $h = 0.09$  Å) at various grid spacings for thioformaldehyde on a domain of union of spheres of radii 5 Å. Dashed and solid lines represent LDA and HF respectively.

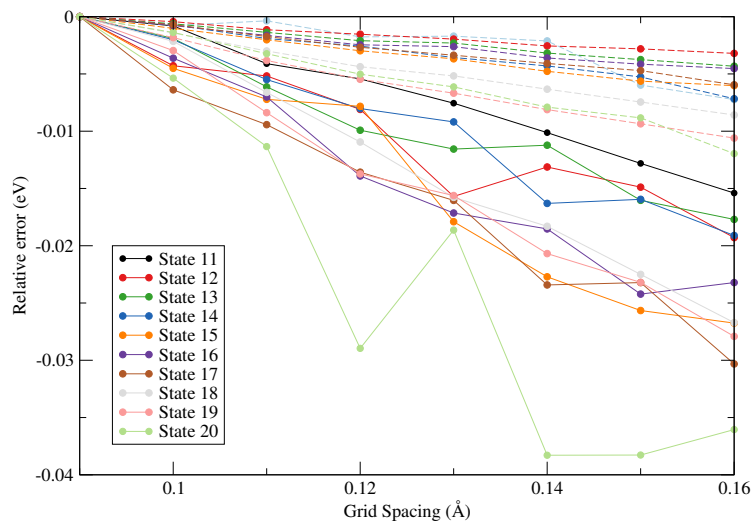


Figure 6: Relative error of the unoccupied orbitals' eigenvalues compared to the finest grid spacing ( $h = 0.09 \text{ \AA}$ ) at various grid spacings for thioformaldehyde on a domain of union of spheres of radii  $5 \text{ \AA}$ . Dashed and solid lines represent LDA and HF respectively.

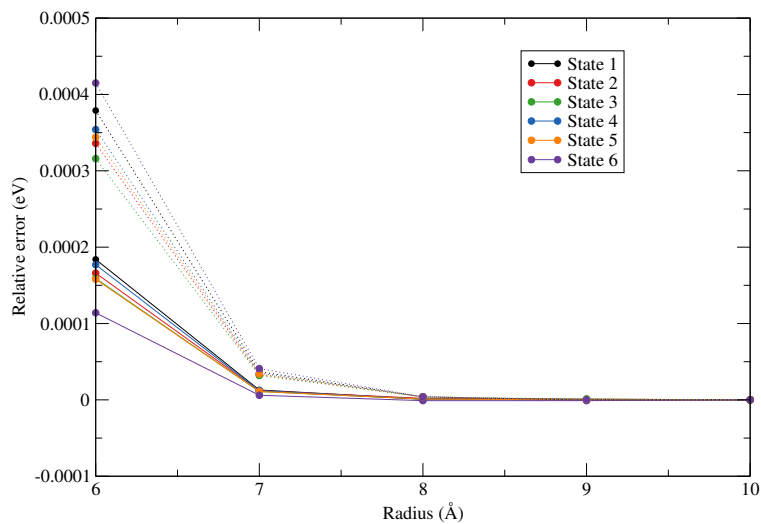


Figure 7: Relative error of the occupied orbitals' eigenvalues compared to the biggest simulation sphere ( $R = 10 \text{ \AA}$ ) at various radii for thioformaldehyde molecule with grid spacing  $h = 0.08 \text{ \AA}$ . Dashed and solid lines represent LDA and HF respectively.

#### 4.5. Benchmarking TDHF

For benchmarking purposes, we’ve chosen to compare our real-space excitation energies from Octopus to those from [50] which uses the GTO code Psi4 [51]. Out of the 17 molecules from the GTO dataset studied there (from [5]), we excluded formaldehyde, methamine and streptocyanine-c1 from our comparison due to problems with convergence of unoccupied levels in real space. We have compared the excitation energies obtained from these two different codes for IPA and TDA from TDDFT using the BLYP functional and also from TDHF.

The unoccupied orbitals and their symmetry is sensitive to the choice of basis set. The number of virtual orbitals obtainable depends on the number of basis functions in GTOs while in real-space it depends on the number of grid-points. For example, using aug-cc-pvtz basis set on acetaldehyde gives 496 basis functions [50], meaning a total of 496 eigenstates can be calculated. But in real-space we are not limited to that number and finer grids give us a larger number of eigenstates. The extra states obtained in real-space calculation are mostly low-lying Rydberg states. This makes the process of targeting the same excitation for comparison in GTO and real-space based approaches difficult. The indices of the states targeted in [50] are different compared to the corresponding ones from real space. The size of the simulation domain also affects the nature of the calculated orbitals. Increasing the domain size results in introduction of new low-lying vacuum states which may not contribute to the absorption spectrum but nonetheless are important in understanding other kinds of response [16]. Figure 8 a) shows the state targeted for the triplet excitation as obtained using GTOs, which is the fourth state after the lowest unoccupied molecular orbital (LUMO). However, in real-space, the same state index represents a Rydberg orbital as shown in figure 8 b). The state resembling the GTO LUMO+4 state is found in real-space as the 30<sup>th</sup> unoccupied state. With this issue in mind, for the comparison of excitation energies against the data from [50], we have ensured that we are targeting the same excitation from both approaches by making sure the symmetry of the unoccupied orbitals matches from both approaches along with their IPA excitation energies. It is harder to determine the symmetry of the orbitals in real space. The symmetry of GTOs can be used to classify orbital symmetries, typically in the solution process. In real space, the Cartesian grid inherently breaks the system’s symmetry in most cases. In this work, we have manually examined the molecular orbitals to determine their irreducible representations.

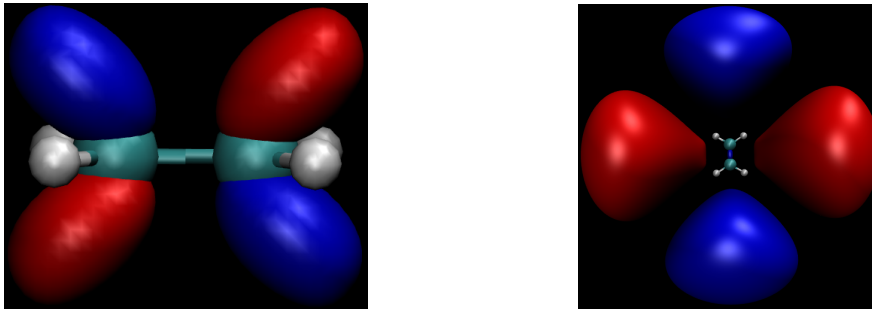
Table 2 summarizes the mean error (ME) and the mean absolute error (MAE) of RS excitation energies as compared to the GTO approach from both TDDFT and TDHF for singlets and triplets. In tables 3 and 4, we show all the triplet and singlet excitation energies, respectively, as obtained from TDDFT (TDBLYP) and TDHF, in the IPA and TDA forms, from both the GTO-based Psi4 code and the real-space (RS) Octopus code. The TBE column represents the “Theoretical Best Estimate” from GTO coupled-cluster calculations in [5]. The singlet energies have a lower overall deviation in real-space while GTOs perform better for triplets. This can be attributed to the cancellation of errors between the two integrals in equation 6. The results are also presented in figures 9 and 10 where as error bars we have depicted the signed deviation from the TBE.

We have also calculated the absorption spectrum using TDHF and compared it against the spectrum from TDDFT. The absorption spectra of the nitrosomethane molecule is shown in figure 11. In addition, to show that these spectra can be successfully and systematically converged, we have shown the absorption spectrum for thioformaldehyde at different grid spacings in figure 12.

## 5. Conclusion

In this work, we have demonstrated a new implementation of linear-response TDHF in the real-space Octopus code, working in the Tamm-Dancoff approximation. For a benchmark set of small molecules, we find good agreement with results from GTOs, though there is a larger

a) GTO Valence LUMO+4 at 2.50 eV    b) Real-space Rydberg LUMO+4 at 1.25 eV



c) Real-space Valence LUMO+29 at 2.82 eV

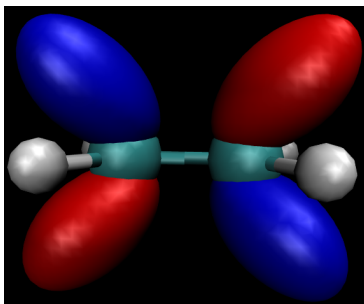


Figure 8: Unoccupied orbitals of ethylene molecule. GTO-based orbital is obtained from Psi4 using aug-cc-pvtz basis set. Real-space orbitals are obtained from Octopus in a simulation sphere with  $R = 10 \text{ \AA}$  and  $h = 0.1 \text{ \AA}$ .

|     | Singlets |      |       |       | Triplets |      |       |      |
|-----|----------|------|-------|-------|----------|------|-------|------|
|     | BLYP     |      | HF    |       | BLYP     |      | HF    |      |
|     | IPA      | TDA  | IPA   | TDA   | IPA      | TDA  | IPA   | TDA  |
| ME  | -0.02    | 0.06 | -0.20 | -0.12 | 0.04     | 0.05 | -0.51 | 0.46 |
| MAE | 0.04     | 0.07 | 0.36  | 0.37  | 0.07     | 0.25 | 0.66  | 1.16 |

Table 2: Mean Error (ME) and Mean Absolute Error (MAE) in eV between real-space (RS) Octopus and Gaussian-type orbital (GTO) Psi4 calculations, for excitation energies from various approaches.

discrepancy for TDHF than for the HF eigenvalues or for TD-BLYP calculations. The source of discrepancies is attributed to the use of semilocal PBE pseudopotentials for our calculations; possible differences in degree of convergence of the RS and GTO calculation; and different treatment of Rydberg excitations – which in general are better described in real space than in GTOs where their energies may be overestimated. Although we have only shown results from RHF here, we have also implemented TDHF for UHF and confirmed that the set of excitation obtained from RHF and UHF are identical for these closed-shell molecules. We find that convergence with respect to the real-space domain’s radius and spacing is harder than for DFT, but still achievable.

Since a linear-response excited-state calculation requires an accurate ground-state calculation first, we examined how to get the HF ground-state in real-space in a practical amount of time. We find that starting with a solution from DFT-LDA as a initial guess instead of LCAO directly from HF speeds up the ground-state convergence considerably. The convergence might not be possible

| Triplets              |                 |      | BLYP       |           |            |           | HF         |           |            |           |
|-----------------------|-----------------|------|------------|-----------|------------|-----------|------------|-----------|------------|-----------|
| Molecule              | Symmetry        | TBE  | IPA<br>GTO | IPA<br>RS | TDA<br>GTO | TDA<br>RS | IPA<br>GTO | IPA<br>RS | TDA<br>GTO | TDA<br>RS |
| acetaldehyde          | A''             | 3.98 | 3.95       | 3.96      | 3.56       | 3.70      | 12.79      | 12.44     | 4.22       | 4.81      |
| acetylene             | A <sub>u</sub>  | 5.56 | 6.66       | 6.71      | 5.85       | 5.00      | 13.68      | 12.37     | 5.41       | 6.49      |
| ammonia               | A''             | 6.37 | 6.52       | 7.03      | 6.50       | 6.94      | 13.02      | 12.39     | 8.64       | 5.76      |
| carbon monoxide       | B <sub>1</sub>  | 6.28 | 7.02       | 6.97      | 5.94       | 6.18      | 17.02      | 15.77     | 5.81       | 9.53      |
| cyclopropene          | B <sub>2</sub>  | 4.38 | 4.97       | 4.97      | 4.10       | 4.31      | 12.19      | 11.57     | 3.52       | 6.30      |
| diazomethane          | A <sub>2</sub>  | 2.80 | 2.90       | 2.91      | 2.59       | 2.70      | 10.10      | 9.29      | 2.33       | 2.00      |
| dinitrogen            | A <sub>u</sub>  | 7.74 | 9.53       | 9.51      | 8.33       | 7.72      | 19.87      | 18.01     | 7.23       | 8.86      |
| ethylene              | B <sub>2u</sub> | 4.54 | 5.60       | 5.61      | 4.54       | 4.79      | 12.76      | 13.08     | 3.61       | 3.27      |
| formamide             | A''             | 5.37 | 5.22       | 5.16      | 4.89       | 4.95      | 12.09      | 12.63     | 5.88       | 5.74      |
| hydrogen sulphide     | A <sub>2</sub>  | 5.74 | 5.69       | 5.64      | 5.34       | 5.43      | 11.83      | 11.13     | 5.59       | 4.83      |
| ketene                | A <sub>2</sub>  | 3.77 | 3.73       | 3.75      | 3.46       | 3.58      | 11.13      | 10.74     | 3.85       | 4.24      |
| nitrosomethane        | A''             | 1.16 | 1.49       | 1.49      | 0.91       | 1.08      | 12.28      | 12.44     | 0.77       | 1.00      |
| thioformaldehyde      | A <sub>2</sub>  | 1.94 | 1.91       | 1.90      | 1.60       | 1.69      | 10.54      | 10.37     | 1.95       | 2.88      |
| water                 | B <sub>1</sub>  | 7.33 | 6.15       | 6.34      | 5.99       | 6.17      | 14.68      | 14.56     | 8.01       | 7.55      |
| Deviation from<br>GTO | ME              |      |            | 0.04      |            | 0.05      |            | -0.51     |            | 0.46      |
|                       | MAE             |      |            | 0.07      |            | 0.25      |            | 0.66      |            | 1.16      |
| Deviation from<br>TBE | ME              |      |            |           | -0.24      | -0.20     |            |           | -0.01      | 0.45      |
|                       | MAE             |      |            |           | 0.38       | 0.31      |            | 0.55      | 0.99       |           |

Table 3: Triplet excitation energies (eV) from TDDFT and TDHF of various molecules, with the irreducible representations given for each excitation. Real-space (RS) results are compared to a GTO dataset [50] for each method, and also to the higher-level theory TBE dataset [5].

| Singlets              |                 |      | BLYP       |           |            |           | HF         |           |            |           |
|-----------------------|-----------------|------|------------|-----------|------------|-----------|------------|-----------|------------|-----------|
| Molecule              | Symmetry        | TBE  | IPA<br>GTO | IPA<br>RS | TDA<br>GTO | TDA<br>RS | IPA<br>GTO | IPA<br>RS | TDA<br>GTO | TDA<br>RS |
| acetaldehyde          | A''             | 4.31 | 3.95       | 3.93      | 4.17       | 4.25      | 12.79      | 12.44     | 5.00       | 4.81      |
| acetylene             | B <sub>2g</sub> | 7.10 | 7.01       | 6.65      | 7.08       | 6.65      | 12.05      | 11.87     | 8.60       | 7.94      |
| ammonia               | A''             | 6.66 | 6.52       | 6.68      | 6.53       | 6.68      | 13.02      | 12.45     | 8.90       | 7.67      |
| carbon monoxide       | B <sub>1</sub>  | 8.48 | 7.02       | 7.01      | 8.39       | 8.59      | 17.02      | 15.76     | 9.00       | 9.53      |
| cyclopropene          | B <sub>1</sub>  | 6.68 | 5.70       | 5.63      | 5.70       | 5.59      | 10.58      | 10.24     | 6.87       | 6.95      |
| diazomethane          | A <sub>2</sub>  | 3.13 | 2.90       | 2.89      | 3.00       | 3.07      | 10.10      | 9.29      | 3.14       | 2.02      |
| dinitrogen            | B <sub>2g</sub> | 9.33 | 8.31       | 8.30      | 9.16       | 9.38      | 18.94      | 18.00     | 9.96       | 9.60      |
| ethylene              | B <sub>3u</sub> | 7.44 | 6.23       | 6.16      | 6.24       | 6.14      | 11.14      | 12.24     | 7.15       | 7.36      |
| formamide             | A''             | 5.63 | 5.22       | 5.19      | 5.39       | 5.44      | 12.09      | 12.63     | 6.53       | 5.92      |
| hydrogen sulphide     | A <sub>2</sub>  | 6.10 | 5.68       | 5.55      | 5.80       | 5.74      | 11.83      | 11.13     | 6.33       | 4.83      |
| ketene                | A <sub>2</sub>  | 3.86 | 3.72       | 3.73      | 3.81       | 3.88      | 11.13      | 10.74     | 4.33       | 4.24      |
| nitrosomethane        | A''             | 1.95 | 1.49       | 1.45      | 1.93       | 2.05      | 12.28      | 11.51     | 2.10       | 2.17      |
| thioformaldehyde      | A <sub>2</sub>  | 2.20 | 1.91       | 1.88      | 2.15       | 2.20      | 10.54      | 10.37     | 2.67       | 2.88      |
| water                 | B <sub>1</sub>  | 7.70 | 6.15       | 6.08      | 6.23       | 6.19      | 14.68      | 14.56     | 8.69       | 7.60      |
| Deviation from<br>GTO | ME              |      |            | -0.02     |            | 0.06      |            | -0.20     |            | -0.12     |
|                       | MAE             |      |            | 0.04      |            | 0.07      |            | 0.36      |            | 0.37      |
| Deviation from<br>TBE | ME              |      |            |           | -0.36      | -0.34     |            |           | 0.62       | 0.21      |
|                       | MAE             |      |            |           | 0.36       | 0.38      |            | 0.66      | 0.58       |           |

Table 4: Singlet excitation energies (eV) from TDDFT and TDHF of various molecules, with irreducible representations given for each excitation. Real-space (RS) results are compared to a GTO dataset [50] for each method, and also to the higher-level theory TBE dataset [5].

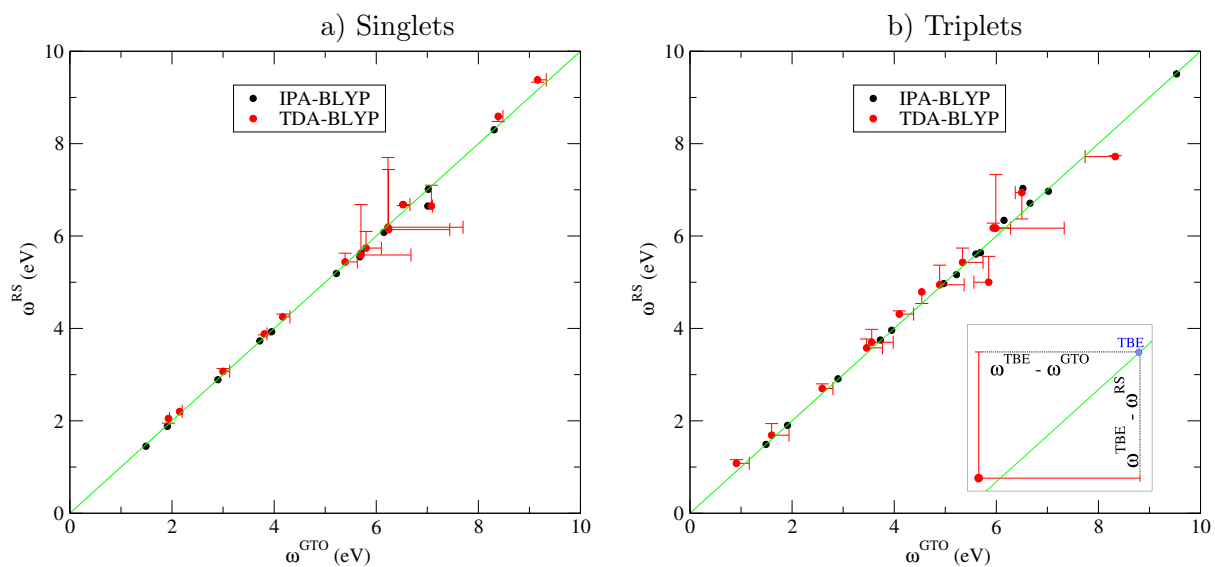


Figure 9: Comparison of TDDFT excitation energies of different molecules from GTOs and real-space. The green line represents the points where  $\omega^{\text{RS}} = \omega^{\text{GTO}}$ .

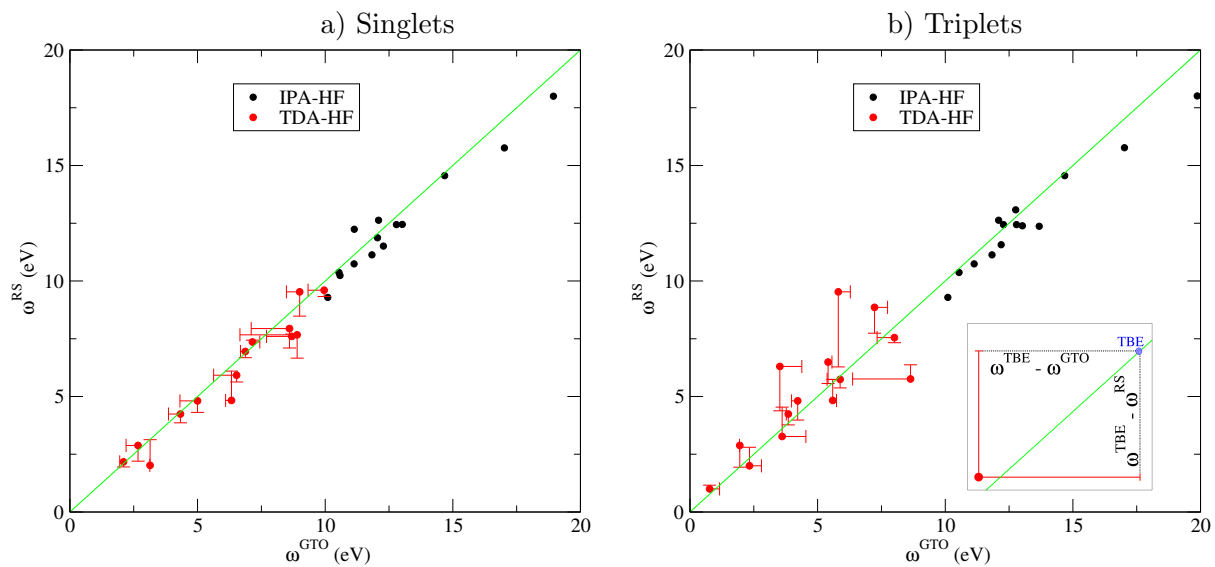


Figure 10: Comparison of TDHF excitation energies of different molecules from GTOs and real-space. The green line represents the points where  $\omega^{\text{RS}} = \omega^{\text{GTO}}$ .



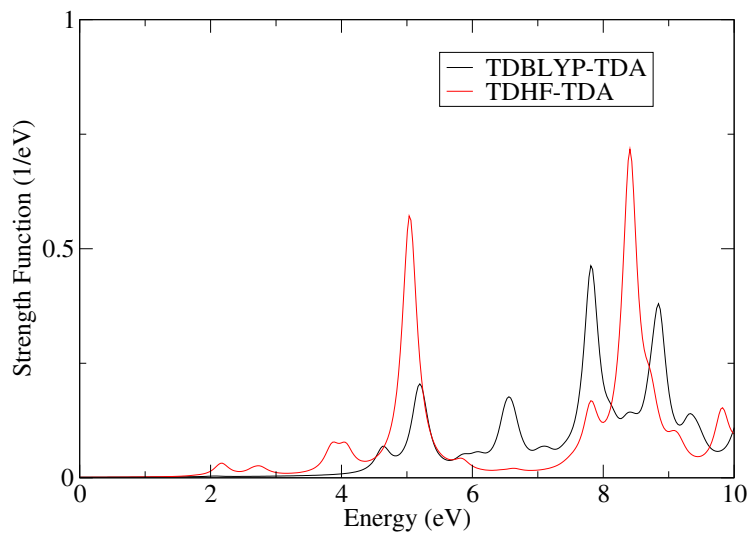


Figure 11: Comparison of singlet absorption spectra of nitrosomethane molecule from TDDFT using BLYP and TDHF. ( $R = 10 \text{ \AA}$ ,  $h = 0.10 \text{ \AA}$  for both TDDFT and TDHF). Lorentzian of width  $0.0136 \text{ eV}$  used for broadening.

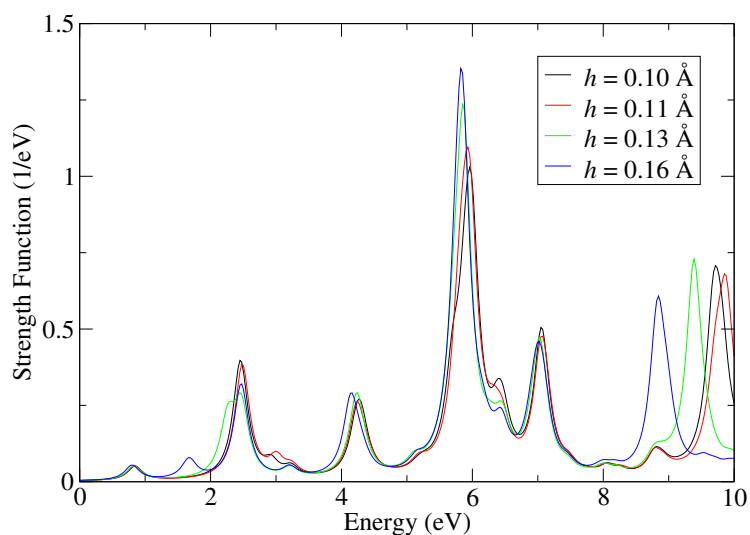


Figure 12: Convergence of triplet absorption spectra of thioformaldehyde molecule with respect to grid spacing from TDHF using TDA, with sphere  $R = 5 \text{ \AA}$ . Lorentzian of width  $0.0136 \text{ eV}$  used for broadening.

at all in some cases without this. We also find that the best way to achieve fast convergence is by mixing states. Linear mixing of potential or density also provides a considerable increase in

the rate of convergence compared to the Broyden scheme, which doesn't seem to facilitate the convergence of the HF ground-state.

The calculation of HF ground-state also requires the calculation of exact exchange which is particularly time-consuming. We have analyzed the use of ACE, an approach to speeding up the exact exchange calculation which can also be used for hybrid DFT. Using the existing implementation of ACE in Octopus, we found that for our benchmark set of molecules, the use of ACE sped up the time per SCF iteration by a factor of 7-14. We also note that the little discrepancy between the results from the two basis choices might be because of the unavoidable use of pseudopotentials in real-space. We have also made sure that the results using ACE match the results without it.

This work adds TDHF to the list of features of the Octopus code, allowing us to compare various approaches in the same platform. We also note that with some further developments to the code, one could include hybrid kernels for TDDFT linear-response calculation now, and also enables use of the TDHF bare-exchange integrals in other theories like ensemble DFT.

## Acknowledgments

We acknowledge Nicolas Tancogne-Dejean for the implementation of ACE in Octopus. This work was supported by the U.S. Department of Energy, Office of Science, Basic Energy Sciences, CTC and CPIMS Programs, under Award DE-SC0019053; Cottrell Scholar Award No. 26921, a program of Research Corporation for Science Advancement; and the UC Merced Academic Senate Faculty Research Grants Program. Computational resources were provided by the MERCED (MRI-1429783) and Pinnacles (MRI-2019144) clusters funded by the National Science Foundation, at Cyberinfrastructure and Research Technologies (CIRT), University of California, Merced.

## References

- [1] Lykos P and Pratt G 1963 *Rev. Mod. Phys.* **35** 496
- [2] Szabo A and Ostlund N S 2013 *Modern Quantum Chemistry: Introduction to Advanced Electronic Structure Theory* Dover Books on Chemistry (Newburyport: Dover Publications)
- [3] Bartlett R J and Stanton J F 1994 Applications of post-Hartree-Fock methods: A tutorial *Reviews in Computational Chemistry* (John Wiley & Sons, Ltd) pp 65–169
- [4] Yu H S, Li S L and Truhlar D G 2016 *J. Chem. Phys.* **145**
- [5] Loos P F, Scemama A, Blondel A, Garniron Y, Caffarelli M and Jacquemin D 2018 *J. Chem. Theory Comput.* **14** 4360–4379
- [6] Becke A D 1993 *J. Chem. Phys.* **98** 1372–1377
- [7] Perdew J P, Ernzerhof M and Burke K 1996 *J. Chem. Phys.* **105** 9982–9985
- [8] Tirado-Rives J and Jorgensen W L 2008 *J. Chem. Theory Comput.* **4** 297–306
- [9] Dreuw A and Head-Gordon M 2005 *Chem. Rev.* **105** 4009–4037
- [10] Hehre W J, Ditchfield R and Pople J A 1972 *J. Chem. Phys.* **56** 2257–2261
- [11] Kim J, Hong K, Choi S, Hwang S Y and Kim W Y 2015 *Phys. Chem. Chem. Phys.* **17** 31434–31443
- [12] Dunning Jr T H and Hay P J 1977 Gaussian basis sets for molecular calculations *Methods of electronic structure theory* (Springer) pp 1–27
- [13] Reislter H and Krylov A I 2009 *Int. Rev. Phys. Chem.* **28** 267–308
- [14] Paterson M J and Townsend D 2020 *Int. Rev. Phys. Chem.* **39** 517–567
- [15] Kendall R A, Dunning Jr T H and Harrison R J 1992 *J. Chem. Phys.* **96** 6796–6806
- [16] Vila F D, Strubbe D A, Takimoto Y, Andrade X, Rubio A, Louie S G and Rehr J J 2010 *J. Chem. Phys.* **133** 034111
- [17] Kronik L, Makmal A, Tiago M L, Alemany M, Jain M, Huang X, Saad Y and Chelikowsky J R 2006 *Phys. Status Solidi B* **243** 1063–1079
- [18] Andrade X, Alberdi-Rodriguez J, Strubbe D A, Oliveira M J T, Nogueira F, Castro A, Muguerza J, Arruabarrena A, Louie S G, Aspuru-Guzik A, Rubio A and Marques M A L 2012 *J. Phys. Condens. Matter* **24** 233202
- [19] Andrade X, Strubbe D A, De Giovannini U, Larsen A H, Oliveira M J T, Alberdi-Rodriguez J, Varas A,

- Theophilou I, Helbig N, Verstraete M J, Stella L, Nogueira F, Aspuru-Guzik A, Castro A, Marques M A L and Rubio A 2015 *Phys. Chem. Chem. Phys.* **17** 31371–31396
- [20] Helbig N, Fuks J I, Casula M, Verstraete M J, Marques M A L, Tokatly I V and Rubio A 2011 *Phys. Rev. A* **83** 032503
- [21] Gygi F and Duchemin I 2013 *J. Chem. Theory Comput.* **9** 582–587
- [22] Casida M and Huix-Rotllant M 2012 *Annu. Rev. Phys. Chem.* **63** 287–323
- [23] Yabana K and Bertsch G F 1996 *Phys. Rev. B* **54**(7) 4484–4487 URL <https://link.aps.org/doi/10.1103/PhysRevB.54.4484>
- [24] Casida M E 1995 Time-dependent density functional response theory for molecules *Recent Advances In Density Functional Methods: (Part I)* (World Scientific) pp 155–192
- [25] Chantzis A, Laurent A D, Adamo C and Jacquemin D 2013 *J. Chem. Theory Comput.* **9** 4517–4525
- [26] Robinson D 2018 *J. Chem. Theory Comput.* **14** 5303–5309
- [27] Kim I, Jeong D, Son W J, Kim H J, Rhee Y M, Jung Y, Choi H, Yim J, Jang I and Kim D S 2023 *npj Comput. Mater.* **9** 81
- [28] Hirata S and Head-Gordon M 1999 *Chem. Phys. Lett.* **314** 291–299
- [29] Perdew J P and Wang Y 1992 *Phys. Rev. B* **45** 13244–13249
- [30] Dirac P A 1930 *Math. Proc. Camb. Philos. Soc.* **26** 376–385
- [31] García-Risueño P, Alberdi-Rodríguez J, Oliveira M J T, Andrade X, Pippig M, Muguerza J, Arruabarrena A and Rubio A 2014 *J. Comput. Chem.* **35** 427–444
- [32] Lin L 2016 *J. Chem. Theory Comput.* **12** 2242–2249
- [33] Damle A, Lin L and Ying L 2015 *J. Chem. Theory Comput.* **11** 1463–1469
- [34] Sharma S, White A F and Beylkin G 2022 *J. Chem. Theory Comput.* **18** 7306–7320
- [35] Jones J R, Rouet F H, Lawler K V, Vecharynski E, Ibrahim K Z, Williams S, Abeln B, Yang C, McCurdy W, Haxton D J, Li X S and Rescigno T N 2016 *Mol. Phys.* **114** 2014–2028
- [36] Colbert D T and Miller W H 1992 *J. Chem. Phys.* **96** 1982–1991
- [37] Brody C G 1965 *Math. Comput.* **19** 577–593
- [38] Johnson D D 1988 *Phys. Rev. B* **38** 12807
- [39] Pulay P 1980 *Chem. Phys. Lett.* **73** 393–398
- [40] Cundari T R and Stevens W J 1993 *J. Chem. Phys.* **98** 5555–5565
- [41] Trail J R and Needs R J 2004 *J. Chem. Phys.* **122** 014112
- [42] Burkatzki M, Filippi C and Dolg M 2007 *J. Chem. Phys.* **126** 234105
- [43] Tan H, Li Y, Zhang S and Duan W 2018 *Phys. Chem. Chem. Phys.* **20** 18844–18849
- [44] Hamann D R 2013 *Phys. Rev. B* **88** 085117
- [45] van Setten M J, Giantomassi M, Bousquet E, Verstraete M J, Hamann D R, Gonze X and Rignanese G M 2018 *Comput. Phys. Commun.* **226** 39–54 <http://www.pseudo-djo.org/>
- [46] Becke A D 1988 *Phys. Rev. A* **38** 3098–3100
- [47] Lee C, Yang W and Parr R G 1988 *Phys. Rev. B* **37** 785–789
- [48] Borlido P, Doumont J, Tran F and Marques M A L 2020 *J. Chem. Theory Comput.* **16** 3620–3627
- [49] Tancogne-Dejean N, Oliveira M J T, Andrade X, Appel H, Borca C H, Le Breton G, Buchholz F, Castro A, Corni S, Correa A A, De Giovannini U, Delgado A, Eich F G, Flick J, Gil G, Gomez A, Helbig N, Hübener H, Jestädt R, Jornet-Somoza J, Larsen A H, Lebedeva I V, Lüders M, Marques M A L, Ohlmann S T, Pipolo S, Rampp M, Rozzi C A, Strubbe D A, Sato S A, Schäfer C, Theophilou I, Welden A and Rubio A 2020 *J. Chem. Phys.* **152** 124119
- [50] Gould T, Hashimi Z, Kronik L and Dale S G 2022 *J. Phys. Chem. Lett.* **13** 2452–2458
- [51] Parrish R M, Burns L A, Smith D G A, Simmonett A C, DePrince III A E, Hohenstein E G, Bozkaya U, Sokolov A Y, Di Remigio R, Richard R M, Gonthier J F, James A M, McAlexander H R, Kumar A, Saitow M, Wang X, Pritchard B P, Verma P, Schaefer III H F, Patkowski K, King R A, Valeev E F, Evangelista F A, Turney J M, Crawford T D and Sherrill C D 2017 *J. Chem. Theory Comput.* **13** 3185–3197